مؤتمر الأزهر الهندسي الدولي العاشر

AL-AZHAR ENGINEERING
TENTH INTERNATIONAL CONFERENCE
December 24 - 26, 2008

Code: M 42

EXPERIMENTAL AND NUMERICAL STUDY FOR OUTWARD FREEZING OF LIQUID-SATURATED POROUS MEDIA IN A VERTICAL ANNULUS

R. Y. Sakr

Mech. Eng. Dept., Faculty of Eng. (Shoubra), Benha Univ.,
108 Shoubra St., Cairo, Egypt, E-mail: rsakr85@yahoo.com

ABSTRACT

Experimental and numerical study is performed to investigate the characteristics of outward freezing heat transfer in water-saturated porous media. Experiments are carried out on a vertical annular space cooled from the inner surface and kept insulated from the outer, lower and upper surfaces. Sandstone grains, glass beads and PVC beads of 16 mm diameter are used as porous media to investigate the thermal conductivity effect on the freezing process. Three different sizes of sandstone grains of average diameters of 4, 8 and 16 mm respectively are used to investigate the effect of the porous matrix.

A mathematical model based on two-dimensional analysis which considered the heat conduction as the only mode of heat transfer in both solid and liquid regions of the PCM. The finite element method is used to develop this model based on Galerkin approach to solve the transient behavior of the freezing in water-saturated porous media phenomenon. Body-fitted curvilinear coordinates are used for treating the freezing front. The effect of thermal conductivity, porosity of the porous media, the wall temperature represented by Stefan number and the initial temperature of liquid phase represented by superheating parameter on the heat transfer characteristics and freezing rate are investigated. Results from the present model have been verified through the comparison with those available in the existing literature and good agreement was observed.

KEYWORDS

Freezing; Porous media; Liquid-saturated; Solid-liquid interface; Phase change material.

1. INTRODUCTION

Solidification of a liquid saturated porous medium occurs in a wide variety of situations in geophysics and engineering. Examples include seasonal freezing of soil, artificial freezing of ground as a construction technique for supporting poor soils, insulation of underground buildings. Metallurgical applications include manufacturing of composite materials and purification of metals. Biomedical applications include cryo-preservation of biological cells

and tissues. Other applications include food processing, nuclear reactor safety, underground burial of radioactive wastes, and latent heat thermal energy storage.

One particular application is the artificial freezing of the ground which is frequently used for construction and mining purposes and recently the method has gained widespread attention in civil engineering practice. The frozen soil is employed as structural support and as a water barrier in large-scale excavations and tunnel or shaft constructions. A series of vertical freezing pipes to produce a line of linked frozen bodies essentially impermeable to ground water flow are used to isolate the saturated region from the underground flow [1]. Predictions of the process of frozen barrier formation and the design of mechanical/thermal systems to produce frozen barrier involves the specification of the equations of fluid flow, heat and mass transport and phase change. These equations are complicated; therefore, most research efforts have studied these equations under simplifying assumptions. Properties such as density, specific heat, and thermal conductivity intimately depend on the characteristics of the porous media (e.g. porosity and permeability). Natural convection, ground water seepage, and other types of fluid flow in the liquid further complicate the phase-change problem.

The solid-liquid phase-change heat transfer problems are called moving boundary problems, in which the unknowns are the interface position that separates the liquid and solid regions as well as the temperature distributions in both regions. The interface motion is determined from the conservation of thermal energy at the interface. This introduces nonlinearity to the problem that has challenged engineers for more than a century since the pioneering study of Stefan on the growth of ice is in 1891. The Stefan model is based on the presence of a sharp interface dividing the whole domain into two subdomains; the unfrozen ice-free and the fully frozen water-free regions. The literature dealing with the freezing of a pure liquid saturated porous medium is abundant and an extensive review is available [2]. A review paper by Sanger [3] examines the applications and other aspects of artificial soil freezing arising in construction. Natural freezing and thawing of soils is important in determining the heat loads of underground buildings. Performance of ground-based heat pumps could be affected by freezing and thawing of the soil around the heat exchanger pipes in the ground [4, 5].

A large part of the available literature has been aimed toward practical design applications used for construction. Sheshukov and Egorov [6] presented a numerical model capable of simulating the freezing of aqueous solution flow in saturated porous media. Their model is based on a finite difference approximation of the coupled equations for liquid water flow, heat and solute transport and phase change. Goldstein and Reid [7] studied freezing or melting in a water-saturated porous medium in the presence of seepage flow. The energy equation in the unfrozen region was solved without knowing the shape of the frozen region. The nonlinear interfacial energy balance was transformed into a nonlinear integral equation which was linearized by solving the equation over short time increments.

Freezing and melting of water in saturated porous media contained in various enclosures had been studied experimentally and numerically by Weaver and Viskanta [8]. Their freezing experiments in a rectangular cavity clearly showed the influence of natural convection on the solid/liquid interface shape and motion. Beckermann and Viskanta [9] combined numerical and experimental studies for solid/liquid phase change in porous media with natural convection in the molten region. Their model was based on volume averaged transport equations, while the phase change was assumed to occur over a small temperature range. Experiments were performed in a vertical, square enclosure using gallium and glass beads as the PCM and the porous matrix, respectively. They showed that natural convection, as well as conduction in the solid, has a considerable influence on the interface shape during both the melting and solidification processes. All these works considered local thermal equilibrium between the solid matrix and the PCM, and this was acceptable because in most of the cases, they are dealing with low thermal conductivity porous media. Chellaiah and Viskanta [10]

conducted an experimental study on freezing of saturated and superheated liquid-porous media contained in a rectangular test cell. The effects of different size glass beads, imposed temperature difference and liquid superheat were investigated. Lein and Richard [11] carried out experiments to visualize the interaction between natural convection and the phase change process in porous media. Various aspect ratios were examined. It was found that the natural convection process is controlled by the mean Rayleigh number and weakens as the freezing process proceeds. An extensive review on multiphase transport in porous media is found in [12]. Mesalhy et al. [13] investigated numerically the melting process inside an irregular geometry filled with high thermal conductivity porous matrix saturated with phase change material PCM. Their model is resting on the averaged conservation equation for mass, momentum and energy with phase change (melting) in porous medium. They found that the best technique to enhance the response of PCM storage is to use a solid matrix with high porosity and high thermal conductivity.

Atwan [14] carried out experiments for inward freezing inside a vertical cylinder containing saturated porous medium. Also, he introduced a mathematical model based on a one dimensional analysis considering the heat conduction as the only mode of heat transfer in both solid and liquid phases using finite difference approximation. Pan and Wu [15] performed a numerical simulation to describe the coupled heat transfer of water saturated soil with a two phase closed thermosyphon using finite difference method. The mechanism of freezing expansion restrained by the two-phase closed thermosyphon is exposed, based on which the effective radius can be determined for engineering applications. Mackie et al. [16] addressed the problem of Rayleigh-Benard instability of a liquid layer undergoing phase transformation within a porous medium. They performed a linear stability analysis which reveals that the onset of convection or the stability of the system is significantly affected by the presence of the porous medium, the state of solidification and the thermal boundary conditions.

It is noticed from the previous literature that only a very limited amount of numerical and experimental investigations on phase-change heat transfer in liquid saturated porous media were available, and understanding of the phenomenon is incomplete. Therefore, the objective of the present work is to investigate experimentally and numerically the thermal characteristics of outward freezing heat transfer in liquid-saturated porous media.

2. EXPERIMENTS

2.1 Experimental Apparatus

The present test apparatus is illustrated schematically in Fig. (1). The main components of the experimental apparatus that built for this research are the test cell which contains the saturated porous media, brine tank which serves as the thermal environment for the freezing experiments and a refrigeration unit for cooling the brine. This apparatus is equipped with devices for circulating, and controlling the brine temperature in its bath, and by appropriate instrumentation.

The brine tank is a polyvinyl chloride (PVC) cylindrical tank with an inside diameter of 500 mm, 800 mm total height, and 15 mm thick. To reduce the heat gain, the tank is insulated with two layers of glass wool with 50 mm thickness. The brine is an aqueous solution of 30-wt% ethylene glycol and is used as the heat transfer fluid. The test cell is connected to the brine tank in which the evaporator of the refrigeration unit is immersed to cool the brine to the desired temperature using a thermostat. In addition, the brine tank is a large reservoir which is selected to smooth any temperature fluctuations associated with cycling. The brine is circulated through the test cell using a 0.5 hp centrifugal pump. The brine flow rate is controlled using valves and measured by an orifice meter with an inverted U-tube manometer. All connecting pipes are PVC and properly insulated to minimize heat gain.

The heart of the experimental apparatus is the test cell in which the outward freezing takes place. The test cell consists of a brass tube of 24 mm outer diameter, 400 mm length and a thickness of 1 mm placed concentrically in a vertical flanged PVC cylinder of 90 mm inner diameter, overall length of 250 mm and 10 mm thickness. The water saturated porous medium is randomly filled in the annular space between the brass tube and the flanged PVC cylinder. The choice of brass thin walled tube being made to facilitate the establishment of the thermal boundary condition for the outward freezing experiments. Two acrylic polystyrene covers of 120 mm diameter and 10 mm thickness are bolted with the flanged PVC cylinder. The test cell is depicted in Fig. (2a).

Measurement of the temperature distribution inside the porous medium was made by three thermocouple racks. Radial and azimuthal positions of the racks are shown in Fig.(2b). The cylinder wall temperature is measured by three thermocouples deployed along the height and around the circumference of the brass cylinder. Two thermocouples are used to measure the brine supply and return temperatures. Another one is used to measure the surrounding temperature. All the thermocouples used are copper-constantan (T-type) having a wire diameter of 0.3 mm and are calibrated prior to their installation in the apparatus. All thermocouple readings are taken using a compensated digital thermometer accurate to 0.1 ^{o}C through selector switches.

2.2 Test Materials

Three types of porous material are tested for outward freezing of saturated water-porous material. These materials are sand grains, glass beads, and PVC beads. The thermophysical properties of the tested materials as well as water and ice are taken from [20], and illustrated in Table (1). This is carried out to show the effect of the thermal conductivity of porous material. The study aimed also to show the effect of grain size or the porosity of the porous medium, so three different sand grain sizes were used. The sand "spheres" are, in fact, not exactly spherical but have a narrow size distribution for which the equivalent diameter is determined from the lower and upper limits of the DIN standard sieving analysis. The sand grains are considered to be spheres of equivalent diameters 4, 8 and 16 mm respectively. The porosity (volume of voids over the total volume) was estimated separately by measuring the volume of water that is needed to fill the void space for a known container volume. Insignificant change in porosity of the particles used of size 8 mm and 16 mm for the three tested materials and its value is about 0.45 while its value for sandstone particles of 4 mm size was 0.4. The discrepancy is due to the roundness of the particles. The packing material was carefully placed into the test cell to ensure uniformity in the structure of the porous matrix. The same packing was used in all experiments. The saturating fluid is the city main water.

Table (1): Thermophysical properties of the test materials, [20]

Property / Material	ρ kg/m^3	Cp J/kg K	k W/m. K
PVC	1380	960	0.15
Glass	2700	800	0.76
Sandstone	2150	710	1.6
Water	1000	4181	0.606
Ice	920	2040	1.88

2.3 Experimental Procedures

The preparations for a freezing run were initiated with the vertical annular container empty and thoroughly clean. To begin, the test cell was first filled with the porous medium. The particles were settled to obtain approximately the same conditions for each run. The ordinary

tap water was carefully siphoned into the test cell to ensure that no air was trapped in the matrix or to prevent air from mixing with the water. Prior to starting each experimental run, the brine is cooled to a temperature below the desired tested wall temperature. Also, the experimental unit is kept at a fixed (reference) temperature. After reaching this initial condition, the experiment starts and the brine begins to circulate through the brass tube that is placed in the middle of the test cell at a suitably chosen flow rates and temperatures (below the fusion temperature). During the run, the porous medium temperatures are recorded at prescribed regular time intervals. From these temperatures, the temperature distributions and solid-liquid interface position as a function of time are determined. The time at which the interface reaches an arbitrary thermocouple (i.e. radial position), is determined as the time when the temperature difference between two consecutive temperature readings can be detected (second reading is below the fusion temperature). Since the temperature readings are taken at finite intervals, this introduces some error in the experimental determination of the solid-liquid interface position.

3. MATHEMATICAL MODEL

3.1 Physical Model and Basic Equations

The physical system for freezing of saturated porous medium contained in the annular space between the inner vertical tube and the outer vertical cylinder is modelled to supplement the experimental results. The annular space is closed at the ends, filled uniformly with solid particles (porous medium) and saturated by water. The top and the bottom of the test cell as well as the outer cylinder are assumed to be adiabatic. Initially, the system is at a uniform temperature greater than or equal to the freezing temperature ($T_i \geq T_f$). At time ($t \geq 0$), a uniform temperature is imposed on the inner tube surface which is less than the freezing temperature, ($T_w < T_f$). This initiates the freezing process with the freezing front moving radially outward. Figure (2) shows the physical model, coordinate system, and thermal boundary conditions. The following assumptions are introduced in the analysis:

1. The porous medium is isotropic and homogeneous.
2. The thermophysical properties are independent of temperature but are different for each phase.
3. The volume change due to phase change is negligible.
4. Two-dimensional heat conduction model is considered in both the solid and the liquid phases, i.e., natural convection in liquid phase is assumed to be absent.
5. The solid-liquid interface is clearly defined, i.e., the PCM has a well-defined phase change temperature.
6. The porosity is uniform.
7. The local thermal equilibrium between phases is assumed.

With the preceding assumptions, the heat transfer process in the liquid and the solid regions are governed by the heat equation which is written in cylindrical coordinates as:

a- for the liquid phase with porous medium;

$$\sigma_{lm} \frac{\partial T_{lm}}{\partial t} = \alpha_{lm} \left(\frac{1}{r} \frac{\partial T_{lm}}{\partial r} + \frac{\partial^2 T_{lm}}{\partial r^2} + \frac{\partial^2 T_{lm}}{\partial z^2} \right) \quad (1)$$

where; $\sigma_{lm} = \frac{(\rho c)_{lm}}{(\rho c)_l}$, $\alpha_{lm} = \frac{k_{lm}}{(\rho c)_l}$

b- for the solid phase with the porous medium;

$$\frac{\partial T_{sm}}{\partial t} = \alpha_{sm}\left(\frac{1}{r}\frac{\partial T_{sm}}{\partial r} + \frac{\partial^2 T_{sm}}{\partial r^2} + \frac{\partial^2 T_{sm}}{\partial z^2}\right) \quad (2)$$

where, (lm) and (sm) refer to the liquid and solid influenced by the porous medium, respectively. These governing equations are subjected to the following initial, boundary, and phase change interface conditions:

$T_{sm}=T_{lm}=T_0$, for $t \le 0$ (initial condition) (3-a)

$T_{sm}=T_w$ at $r = r_i$ (at inner surface) (3-b)

$T_{sm}=T_{lm}=T_f$ at $r = r^*(z,t)$ (at solid-liquid interface) (3-c)

$\frac{\partial T_{lm}}{\partial r} = 0$ at $r=r_o$ (at the outer surface) (3-d)

$\frac{\partial T_{sm}}{\partial z} = \frac{\partial T_{lm}}{\partial z} 0$ at z=0, z=H (at the bottom and the top surfaces) (3-e)

Also, another condition at the solid liquid interface is obtained by applying the energy balance at the solid-liquid interface, at which the heat conducted to the interface from the liquid is equated to the latent heat required by the phase change plus the conduction into the solid, which may be written as:

$$q_{lm} = q_s + q_{sm}$$

where, q_s is the energy released to solidify a layer of thickness δr which is per unit surface area is;

$$q_s = \varepsilon \rho_s \Delta h_f \frac{\partial r^*}{\partial t}$$

Therefore, the interfacial energy balance yields;

$$\left[1+\left(\frac{\partial r^*}{\partial z}\right)^2\right]\left(k_{sm}\frac{\partial T_{sm}}{\partial r} - k_{lm}\frac{\partial T_{lm}}{\partial r}\right) = \varepsilon\rho_s \Delta h_f \frac{\partial r^*}{\partial t} \quad (3\text{-f})$$

It is noted that the difference in density of the solid and liquid PCM is accounted for the interfacial energy balance, but is neglected in the energy equation (i.e. convection is absent).

3.2 Coordinate Transformation and Dimensionless Governing Equations

The main feature of the freezing/melting problems is the geometrical change and movement of the irregular solid-liquid interface and the non-linearity associated with the solid-liquid interface. This makes the problem to be highly non-linear. One resolution of former difficulty is to perform an immobilization transformation of coordinates. This simplifies the numerical analysis by transforming the irregular boundary to a fixed one of much simpler geometry, at the expense of complicating the governing equations, so the problem of discretization at each time step is avoided. The formulation of the irregular front motion and the determination of its location requires two spatial coordinates. Introducing the general Oberkampf transformation [17] as follows:

$$\xi = \frac{r - r_l(z)}{r_u(z) - r_l(z)}, \quad \eta = \frac{z - z_l(r)}{z_u(r) - z_l(r)} \quad (4)$$

Applying the above expressions for both solid-porous medium phase and liquid-porous medium phase respectively, selecting the domain height H as a reference length and selecting the following non dimensional groups:

$$R^* = \frac{r^*(z,t)}{H},\quad \mathrm{R_i} = \frac{r_i}{H}, \mathrm{R_o} = \frac{\mathrm{r_o}}{\mathrm{H}},\ \theta = \frac{T_{sm} - T_f}{T_f - T_w},\quad \mathrm{Fo} = \frac{\alpha_{\mathrm{sm}} t}{H^2},\ \mathrm{Ste}^* = \frac{\mathrm{c_{sm}}\left(T_f - T_w\right)}{\Delta \mathrm{h_f}}$$
$$\mathrm{Ste} = \frac{\mathrm{c_s}\left(T_f - T_w\right)}{\Delta \mathrm{h_f}},\ \tau = \mathrm{Fo.Ste}^*, \mathrm{k}^* = \frac{\mathrm{k_{lm}}}{\mathrm{k_{sm}}},\ \mathrm{Sc} = \frac{T_0 - T_f}{T_f - T_w},\ \delta_{\mathrm{sm}} = R^* - R_i,\ \delta_{\mathrm{lm}} = \mathrm{R}_o - \mathrm{R}^* \tag{5}$$

where, Ste^* is the solid phase-porous media Stefan number, and other symbols are as defined in the nomenclature. With the preceding dimensionless variables, the resulting dimensionless immobilized transformed energy equations for both the solid and the liquid phases influenced by the porous medium are, respectively,

For the solid,

$$\frac{\partial \theta_{sm}}{\partial Fo} = \left\{ \begin{array}{l} \left(\dfrac{\xi^2}{\delta_{sm}^2}\left(\dfrac{\partial R^*}{\partial \eta}\right)^2 + \dfrac{1}{\delta_{sm}^2}\right)\dfrac{\partial^2 \theta_{sm}}{\partial \xi^2} - \dfrac{2\xi}{\delta_{sm}}\left(\dfrac{\partial R^*}{\partial \eta}\right)\dfrac{\partial^2 \theta_{sm}}{\partial \xi \partial \eta} + \dfrac{\partial^2 \theta_{sm}}{\partial \eta^2} \\ \left(\dfrac{1}{\xi \delta_{sm} + R_i \delta_{sm}} - \dfrac{\dot{R}^* \xi}{\delta_{lm}} - \dfrac{\xi}{\delta_{lm}}\dfrac{\partial^2 R^*}{\partial \eta^2} + \dfrac{2\,\xi}{\delta_{sm}^2}\left(\dfrac{\partial R^*}{\partial \eta}\right)^2\right)\dfrac{\partial \theta_{sm}}{\partial \xi} \end{array} \right\} \tag{6}$$

For the liquid,

$$\sigma_{lm}\frac{\partial \theta_{lm}}{\partial Fo} = \left\{ \begin{array}{l} \left(\dfrac{(\xi-1)^2}{\delta_{lm}^2}\left(\dfrac{\partial R^*}{\partial \eta}\right)^2 + \dfrac{1}{\delta_{lm}^2}\right)\dfrac{\partial^2 \theta_{lm}}{\partial \xi^2} + \dfrac{2(\xi-1)}{\delta_{lm}}\left(\dfrac{\partial R^*}{\partial \eta}\right)\dfrac{\partial^2 \theta_{lm}}{\partial \xi \partial \eta} + \dfrac{\partial^2 \theta_{lm}}{\partial \eta^2} \\ \left(\dfrac{1}{\xi \delta_{lm}^2 + R^* \delta_{lm}} - \dfrac{\alpha_{lm}\dot{R}^*(\xi-1)}{\delta_{lm}} + \dfrac{(\xi-1)}{\delta_{lm}}\dfrac{\partial^2 R^*}{\partial \eta^2} + \dfrac{2(\xi-1)}{\delta_{lm}^2}\left(\dfrac{\partial R^*}{\partial \eta}\right)^2\right)\dfrac{\partial \theta_{sm}}{\partial \xi} \end{array} \right\} \tag{7}$$

Also, the initial, boundary, and interface conditions, Eq. (3), may be given in a dimensionless form as:

$\theta_{lm}=\theta_0$, for $\tau \le 0$ (initial condition) (8-a)

$\theta_{sm}=\theta_w=-1$ at $\xi_1 = 0$ (at inner surface) (8-b)

$$\frac{\partial \theta_{lm}}{\partial \xi} = 0 \quad \text{at } \xi_2 = 1 \quad \text{(at outer surface)} \tag{8-c}$$

$$\frac{\partial \theta_{sm}}{\partial \eta} = \frac{\partial \theta_{lm}}{\partial \eta} = 0 \quad \text{at } \eta=0,\ \eta=1 \quad \text{(at the lower and the upper surfaces)} \tag{8-d}$$

$\theta_{sm}=\theta_{lm}=0$ at $\xi_1 = 1$, $\xi_2 = 0$ (at solid-liquid interface) (8-e)

$$\left(1 + \left(\frac{\partial R^*}{\partial \eta}\right)^2\right)\left(\frac{\partial \theta_{sm}}{\partial \xi} - k^* \frac{\delta_{sm}}{\delta_{lm}}\frac{\partial \theta_{lm}}{\partial \xi}\right) = \frac{\delta_{sm}\rho_s \varepsilon}{\rho_{sm} Ste^*}\frac{\partial R^*}{\partial Fo} \text{ (at solid-liquid interface)} \tag{8-f}$$

Before the model equations can be solved, a viable means of determining the thermophysical properties of the porous media is needed. Effective or average properties are used which are based on the fraction of each constituent. Specially, the effective density, specific heat, and thermal conductivity, which results in the following equations for the solid and the liquid phases influenced by the porous media.

$$\rho_{sm} = \varepsilon\, \rho_s + (1-\varepsilon)\rho_m \tag{9-a}$$

$$c_{sm} = \varepsilon\, c_s + (1-\varepsilon) c_m \tag{9-b}$$

$$k_{sm} = \varepsilon\, k_s + (1-\varepsilon) k_m \tag{9-c}$$

$$\rho_{lm} = \varepsilon\, \rho_l + (1-\varepsilon) \rho_m \tag{9-d}$$

$$c_{lm} = \varepsilon\, c_l + (1-\varepsilon) c_m \tag{9-e}$$

$$k_{lm} = \varepsilon\, k_l + (1-\varepsilon) k_m \tag{9-f}$$

where, s, l, and m, respectively, refer to the solid phase of PCM, the liquid phase of PCM, and the porous medium.

3.3 Numerical Solution and Finite Element Formulation

The finite element analysis is presented here for the transformed basic equations using linear triangular elements. Equations (6) and (7) with the appropriate boundary conditions of Eqs. (8) are formulated using the Galerkin based finite element method [18, 19]. The objective of the finite element is to reduce the system of governing equations into a discretized set of algebraic equations. The procedure begins with the division of the continuum region G, of interest (computational domain) into a number of simply shaped regions (triangles) called finite elements.

The Finite Element Formulation

The temperature, for either the solid or the liquid induced saturated porous media in any element (triangle) of the discretized domain can be represented in terms of nodal temperature by the following simple polynomials:

$$\theta^e = \sum_{m=1}^{3} N_m \theta_m \tag{10}$$

where;

$$N_1 = \frac{1}{2A}(a_1 + b_1\xi + c_1\eta) \tag{11-a}$$

$$N_2 = \frac{1}{2A}(a_2 + b_2\xi + c_2\eta) \tag{11-b}$$

$$N_3 = \frac{1}{2A}(a_3 + b_3\xi + c_3\eta) \tag{11-c}$$

where;

A = area of the triangle element 123

$$a_1 = \xi_2\eta_3 - \xi_3\eta_2 \qquad a_2 = \xi_3\eta_1 - \xi_1\eta_3 \qquad a_3 = \xi_1\eta_2 - \xi_2\eta_1$$

$$b_1 = \eta_2 - \eta_3 \qquad b_2 = \eta_3 - \eta_1 \qquad b_3 = \eta_1 - \eta_2$$

$$c_1 = \xi_3 - \xi_2 \qquad c_2 = \xi_3 - \xi_1 \qquad c_3 = \xi_1 - \xi_3$$

The interpolation functions [N_1, N_2, N_3] in Eqs. (11) are derived from the assumption of linear variation of temperature in the element. The approximate expressions of the system variables are substituted into the governing equations (6) and (7) and the global errors are minimized using the above interpolation functions N_i (i = 1, 2, 3) as weighting functions. The solution of Eqs. (5) and (6) that satisfies the boundary conditions given by Eqs. (8) can be obtained after weighted integration over the domain G^e and the application of Green's theorem, in the equivalent matrix form. Then, these equations can be assembled to obtain the global characteristic matrix and the global characteristic vector. The system matrices on the global level can be written in the form:

$$[K]_I \{\theta\} + [K_C]_I \{\dot{\theta}\} = \{F\}_I, \quad \text{for the solid phase induced porous medium} \tag{12-a}$$

$$[K]_{II} \{\theta\} + [K_C]_{II} \{\dot{\theta}\} = \{F\}_{II}, \quad \text{for the liquid phase induced porous medium} \tag{12-b}$$

where,
$[K]_I$ and $[K]_{II}$ are the global stiffness matrices.
$[K_C]_I$ and $[K_C]_{II}$ are the global heat capacity matrices.
$\{F\}_I$ and $\{F\}_{II}$ are the global force vector
The above matrices are derived from the followings:

A common procedure is to solve the time dependent model equations and thus obtain the values of the unknown variable at each point in time, so, the final form of equations on the global level, which are used to solve for the unknown variable at time, Fo, are given as:

$$\left[K^*\right]\left\{\theta_{Fo}\right\} = \left\{F^{*`}\right\} \tag{13}$$

where;

$$\left[\mathrm{K}^*\right] = \left[\mathrm{K_C}\right]_{\mathrm{Fo}} / \Delta\mathrm{Fo} + \left[\mathrm{K}\right]_{\mathrm{Fo}}$$

$$\left\{\mathrm{F}^*\right\} = \left\{\mathrm{F}\right\}_{\mathrm{Fo}} + \left(\left[\mathrm{K_C}\right]_{\mathrm{Fo}} / \Delta\mathrm{Fo}\right)\left\{\theta_{\mathrm{Fo}-\Delta\mathrm{Fo}}\right\}$$

and

$$[\mathrm{K}^*] = \sum_{e=1}^{E} \int_{G^e} \left(\frac{\partial[\mathrm{N}]^T}{\partial\xi} \cdot \frac{\partial[\mathrm{N}]}{\partial\xi} + \frac{\partial[\mathrm{N}]^T}{\partial\eta} \cdot \frac{\partial[\mathrm{N}]}{\partial\eta} \right) \mathrm{dG}$$

$$\{\mathrm{F}^*\} = \sum_{e=1}^{E} \int_{\Gamma^e} \left([\mathrm{N}]^T \frac{\partial \mathrm{T}}{\partial\xi} + [\mathrm{N}]^T \frac{\partial \mathrm{T}}{\partial\eta} \right) \mathrm{d}\Gamma$$

where;

E = total number of elements, G bounded computational domain,

Γ domain boundary, and

$\{\theta_{Fo}\}$, $\{\theta_{Fo-\Delta Fo}\}$ are the nodal matrices of the unknown variable which is the temperature is the solid phase and the liquid phase induced porous media respectively. Equation (13) gives a set of linear equations which have been solved by Gauss elimination method. The finite element formulation and the resulting linear equations were solved through a computer program written here in FORTRAN code.

3.4 Model Validation

The accuracy of the numerical procedure employed in the present study is validated through the comparison with the experimental data of Mohamed [21] for the limiting case of a homogeneous medium (no porous medium ε=1) as shown in Fig. (4). The present numerical results obtained for ice growth layer (solidified layer thickness) are found to be in good agreement with this experimental data for freezing of water around a vertical cylinder.

4. RESULTS AND DISCUSSIONS

4.1 Experimental Results

Experiments are carried out to investigate the governing parameters on the freezing process of the liquid saturated porous media. Three materials, PVC beads, glass beads and sandstone grains are tested with tap water as a saturating fluid to simulate different types of soils. The operating conditions are characterized by the subcooling of the inner tube wall temperature below the phase change temperature is represented by either Stefan Ste or modified Stefan Ste^* number and the initial liquid phase superheating represented by the superheating coefficient Sc that are defined in Eq. (5).

During the freezing process, the solid-liquid interface location, consequently the freezing rate and the temperature distribution in both solid and liquid phases are unknowns; therefore, our discussions will concentrate on these unknowns. The timewise variation of the temperature at different radial distances for all test media is shown in Figs. (5-7). It is observed from the figure that the temperature is rapidly decreases at the early stages of the freezing process due to the sensible heat librated from the superheated liquid and the later reaches the freezing temperature. The solid region is represented by the portion of the temperature distribution below the freezing temperature (T_f=0), even though the freezing process of water takes place within a certain temperature range because of salts and impurities in water.

As the solidified layer thickness increases, the freezing rate decreases due to the increase of the thermal resistance to heat flow from liquid phase to the inner cold brass tube. At later stages of the freezing process the temperature distribution becomes horizontal having temperature values near the tube wall temperature. It is also noticed that the temperature distribution is strongly affected by the effective thermal conductivity i.e. higher effective thermal conductivity gets narrower range of temperature variation.

The timewise variation of the temperature at different axial locations at nearly the mid vertical plane of the annulus layer (r=27 mm) for water saturated-sandstone grains is depicted in Fig. (8). The figure shows that the temperature distribution is slightly affected by the axial location. The same behaviour is also noticed for both glass and PVC beads and is not shown for sake of brevity.

4.2 Numerical Results

To supplement the experimental work and cover a wide range of the governing parameters a series of numerical runs are performed. This is done in order to illustrate the effect of various parameters, e.g. initial liquid phase induced porous medium temperature represented by superheating coefficient Sc, cold wall temperature which represented by Stefan or modified Stefan number, porosity or void fraction, and porous medium material type on the freezing process of water saturated porous media. Decreasing the initial liquid temperature means decreasing the superheating coefficient. The effect of superheating coefficient on the freezing process of glass beads of ε=0.45 is illustrated in Fig. (9). It is noticed from the figure, as the superheating coefficient decreases the freezing rate increases. This is attributed to higher net heat flux at the solid-liquid interface and consequently higher freezing rate.

The effect of wall temperature is represented by Stefan or modified Stefan number effect. Decreasing the wall temperature is equivalent to increasing Stefan or modified Stefan number which results in increasing the freezing rate of water saturated-glass beads as shown in Fig. (10). It is observed from the figure that the slop of all curves is high and approximately the same due to the rapid growth of the solidified layer at the earlier time. With time progressing, the frozen layer thermal resistance increases and this means lower freezing rate. The effect of the porosity on the freezing rate is depicted in Fig. (11), for sandstone grains at superheating coefficient Sc=2.5. It is observed from the figure that as the porosity increases the freezing rate decreases and this is due to the decrease of the effective thermal conductivity and more energy is required to be removed to solidify more water that occupies voids. The timewise variation of the frozen volume fraction for water saturated sandstone, glass and PVC beads is illustrated in Fig. (12). Higher freezing rate for sandstone grains is observed due to higher effective thermal conductivity. The dimensionless time is replaced by the time in minutes as it is a function of the thermal diffusivity and gets confusion.

Figure (13) shows the timewise variation of the dimensionless temperature at three different radial locations in the liquid saturated PVC beads phase denoted by ξ_2= 0.25, 0.5, and 0.75 respectively at an axial location denoted by η_2=0.6. From the figure, it is illustrated that all the locations started from the initial dimensionless temperature having a value of 0.5 and finished

with zero value corresponding to the freezing point. Also, the nearer is location from the cold inner tube the lower is the temperature. The dimensionless temperature at different axial locations in the liquid saturated PVC beads denoted by η_2=0.25, 0.6 and 0.9 respectively at a radial location denoted by ξ_2=0.5 is illustrated in Fig. (14). The figure shows lower temperature is attained at the mid-height of the annulus indicating more freezing rate than the lower and higher levels of the annulus.

The predicted freezing front locations for water saturated PVC beads, glass beads, and sandstone grains are illustrated in Fig. (15) at ε=0.45, Sc=2.5. It is observed from the figure that the intensity of lines is higher for PVC indicating that more time intervals are required for freezing the same volume and this is due to its lower thermal conductivity. The temperature contours for the water saturated sandstone grains undergoing freezing process at t=30, 90 and 150 minutes respectively are illustrated in Fig. (16).

The model predictions of the frozen volume fraction illustrated in Figs (9-12) are utilized to obtain the following correlation equation:-

$$\frac{V}{V_o} = 4.927\ \tau^{0.523} Sc^{-0.176} k^{*-0.388} \varepsilon^{-0.776} \qquad (14)$$

where;

$1.56x10^{-5} \le \tau \le 1.16x10^{-2}$, $1.25 \le Sc \le 5$, $0.546 \le k^{*} \le 0.773$, and $0.3 \le \varepsilon \le 0.6$ with a maximum deviation of 6 %.

4.3 Comparison of Present Predictions with Experimental Data

In comparing the predictions of the numerical model with the experimental data, a sample of results is used for sake of brevity. Figure (17) illustrates the temperature distributions at different times during the freezing process of water saturated-sandstone grains of average particle size of 16 mm diameter at an axial location denoted by $\eta_1=\eta_2$=0.6. The figure indicates that there are some discrepancies especially in solid phase induced porous medium. This is attributed to temperature dependent thermophysical properties, variation in the inner tube wall temperature that takes place during the experiments and contact resistance that are not considered in the model. The same behaviour is noticed for the freezing process of water saturated PVC beads in Fig. (18).

The comparison of the prediction with experimental data for the frozen volume fraction at different times for the freezing process of water saturated sandstone grains and PVC bead is shown in Fig. (19). Good agreement between the prediction and the experimental data is observed.

Based on the experimental data presented in Fig. (19) as well as experimental data for frozen volume fraction of sandstone grain of average diameters of 4 mm and 8 mm, the following empirical correlation equation was obtained:

$$\frac{V}{V_o} = 245.2\ \tau^{1.1} Ste^{*0.174} \qquad (15)$$

where; $7.7x10^{-4} \le \tau \le 8.17x10^{-3}$, $0.0373 \le Ste^{*} \le 0.0664$ with a maximum deviation of 15 %.

5. CONCULSIONS

From the findings in the present work, the following concluding remarks are obtained:

1. The freezing process of water saturated-porous media is controlled mainly by either controlling the effective thermophysical properties of the porous matrix or the initial and operating conditions.

2. The freezing rate of water saturated-sandstone grains is higher than that of water saturated-glass and PVC beads due to its higher effective thermal conductivity.
3. The freezing rate increases with either decreasing the superheating coefficient (decreasing the initial media temperature) or increasing Stefan number (decreasing the cold tube wall temperature).
4. A computer code, based on two-dimensional heat conduction model is developed and predicts reasonably the temperature field in both solid and liquid phase induced porous media as well as the freezing rate of water that saturates the porous media.
5. The discrepancy between the experimental data and predictions is in general attributed to the temperature dependent thermophysical properties of the test materials, change in density which accompanies phase change, the variation of inner tube wall temperature during the time of the experiments, as well as the thermal resistance between the wall and the media.
6. Correlation equations for the frozen volume fraction as a function of different operation parameters are obtained.

REFERENCES

1. Grant S, Iskander I.K., Artificially Frozen Ground as a Subsurface Barrier Technology. In: Summary of Workshop, Barrier Technologies for Environmental Management. Washington: National Academy Press, 1997, p.D153-60.
2. R. Viskanta, Phase Change Heat Transfer in Porous Media, in Z.P. Zarling (Ed.), Third International Symposium on Cold Regions Heat Transfer, University of Alaska, Fairbanks, AK, 1991, pp.1-24.
3. Sanger, F. J., "Ground Freezing in Construction", ASCE Mechanics and Foundations Division, Vol. 94, pp. 131-158, 1968.
4. Mertz, P. D., "A simple Computer Program to Model Three-Dimensional Underground Heat Flow With Realistic Boundary Conditions", ASME Journal of Solar Energy Engineering, Vol. 105, pp.42-49, 1983.
5. Svec, O., Goodrich, L. E., and Planar, J. H. L., "Heat Transfer Characteristics of In-Ground Heat Exchangers", Journal of Energy Research, Vol. 7, pp. 263-278, 1983.
6. Sheshukov, Y.Y. and Egorov, A.G., "Frozen Barrier Evolution in Saturated Porous Media," Advances in Water Resources, Vol. 25, pp. 591-599, 2002.
7. Goldstein, M. E., and Reid, R. L., "Effect of Fluid Flow on Freezing and Thawing of Saturated Porous Media", Proceedings of the Royal Society of London, Series A, Vol. 364, pp. 45-73, 1978.
8. Weaver, J. A., and Viskanta, R., "Freezing of Liquid-Saturated Porous Media", ASME Journal of Heat Transfer, Vol. 108, pp. 654-659, 1986.
9. Beckermann C., and Viskanta, R., "Natural Convection Solid-Liquid Phase Change in Porous Media," Int. J. Heat Mass Transfer, Vol. 31, pp. 35-46, 1988.
10. Chellaiah, S., and Viskanta, R., "Freezing of Saturated and Superheated Liquid in Porous Media", Int. J. Heat Mass Transfer, Vol. 31, pp. 321-330, 1988.
11. Lein, H. T., and Richard, S.," Natural Convection in in Porous Media. II. Freezing", Int. J. Heat Mass Transfer, Vol. 35, pp. 187-194, 1992.
12. Eaton, R.R., Kaviany, M., Sharma, M. P. Udell, K. S., and Vafai, K." Proceedings of the 1993 ASME Winter Annual Meeting", Multiphase Transport in Porous Media, ASME, Fluids Engineering Division, New York, Vol. 173, 155p., 1993

13. Osama Mesalhy, Khalid Lafdi, Ahmed Elgafy and Keith Bowman, "Numerical Study for Enhancing the Thermal Conductivity of Phase Change Material (PCM) Storage Using High Thermal Conductivity Porous Matrix," Energy Conversion and Management, Vol. 45, pp. 847-867, 2005.
14. Atwan, E.F., "Experiments and Numerical Simulations for Freezing of Liquid-Saturated Porous Media," 2nd Int. Conference on Advances in Engineering Science & Technologies, Paper No. ME 30
15. Pan, Y. and Wu, C., "Numerical Investigations and Engineering Applications on Freezing Expansion of Soil restrained Two-Phase Closed Thermosiphons," Int. J. Thermal Science, Vol. 41, pp. 341-347, 2002.
16. Mackie, C., Desai, P. and Meyers, C., "Rayleigh-Benard Stability of a Solidifying Porous Medium," Int. J. Heat Mass Transfer, Vol. 42, pp. 3337-3350, 1999.
17. Oberkampf, W.I., "Domain Mapping for the Numerical Solution of the Partial Differential Equations," Int. J. for Numerical Methods in Engineering, pp. 211-223, 1976.
18. Zienkiewicz, O.C. and Taylor, R.L., Finite Element Method, Fifth edition, Butterworth, Heinmann, 2000.
19. Lewis, R.W., Nithiarasu, P., Seetharamu, K., Fundamentals of the Finite Element Method for Heat and Fluid Flow, John Wiley & Sons, 2004.
20. Adrian Bejan, and Allan D. Kraus., Heat Transfer Handbook, John Wiley& Sons, 2003.
21. Mohamed, M.M., "Solidification of Phase Change Material on Vertical Cylindrical Surface in Holdup Air Bubbles," Int. J. of Refrigeration, Vol. 28, pp. 403-411, 2005.

NOMENCLATURE

SI system of units is used for the whole parameters within the present paper.

A element area
$a_1,b_1,c_1,..$ polynomial coefficients, Eq. (11)
c specific heat
d bead mean dimeter
{F} force vector, Eq. (12).
G computational domain
Δh_f latent heat of fusion
k thermal conductivity
[K] stiffness matrix
$[K_C]$ heat capacity matrix
N interpolation function
q heat flux
r_o outer radius of the bed
r radial, position or coordinate
r^* front location
T temperature
t time
V frozen volume fraction
V_o initial volume
z axial coordinate

Subscripts:

0 initial
f front or fusion
i nodal point number or inner
l liquid phase or lower
sm solid phase influenced by porous medium
u upper
w wall
e element level

Superscripts:

n previous time
n+1 current time
* interface position

Greek letters:

α thermal diffusivity ($k/\rho c$)
Δ incremental step
ε average void fraction
ξ,η immobilized transformed coordinates

Dimensionless terms:

Fo Fourier number ($\alpha_{sm}\, t / H^2$)
k^* effective thermal conductivity ratio, Eq. (5).
R dimensionless radial distance (r/H)
R^* dimensionless interface position (r*/H)
Sc liquid superheating coefficient, Eq. (5).
Ste^* modified Stefan number, Eq. (5).
Ste Stefan number, Eq. (5).
δ dimensionless frozen and unfrozen layer
σ given by Eq. (1).

lm liquid phase influenced by porous medium
m porous medium
o outer
s solid phase

θ dimensionless temperature
τ dimensionless time, (Fo.Ste*)

Abbreviations:
PCM phase change material
PVC polyvinyl chloride

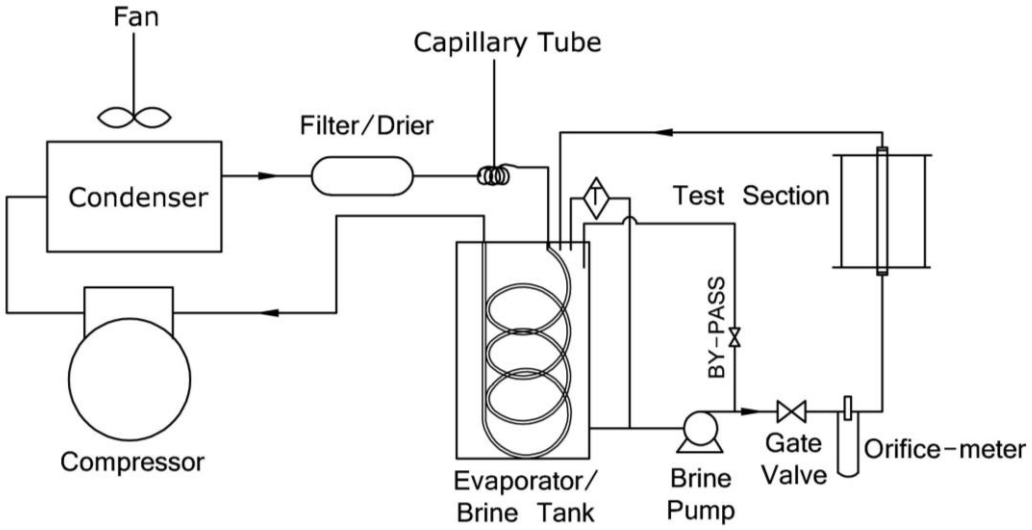

Fig. (1): Schematic diagram of the experimental set-up

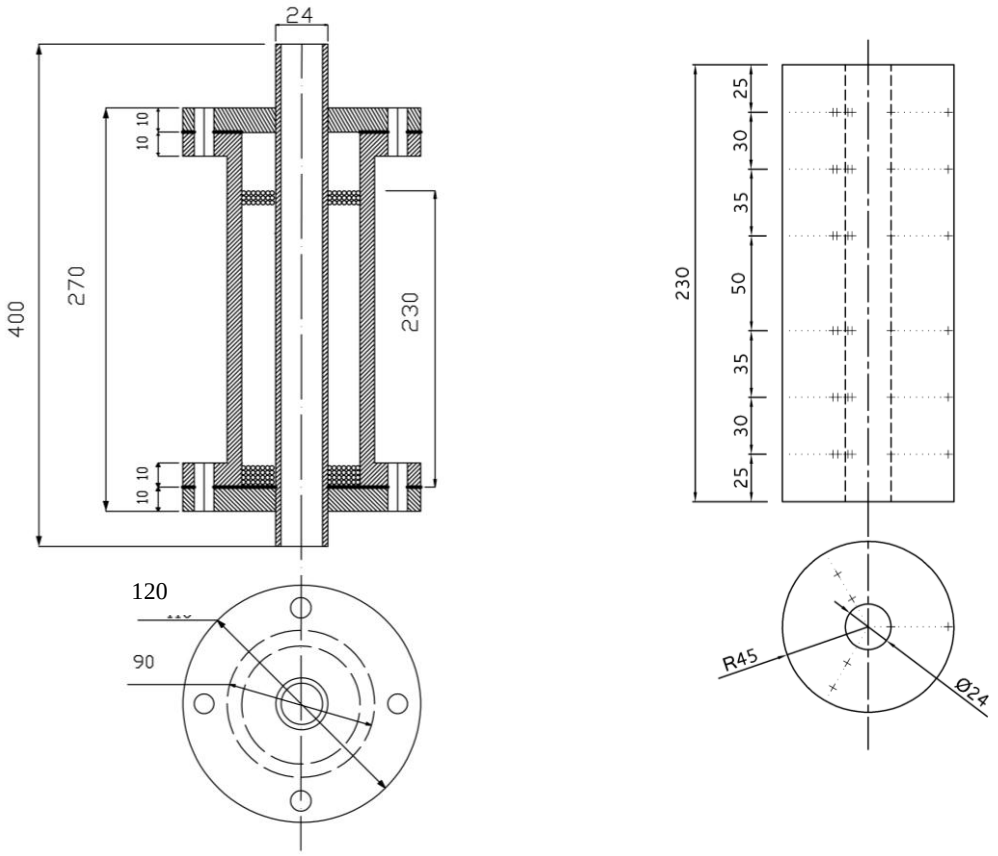

(a) Test cell (b) Thermocouples locations

Fig. (2): Schematic diagram of the test cell and thermocouple locations

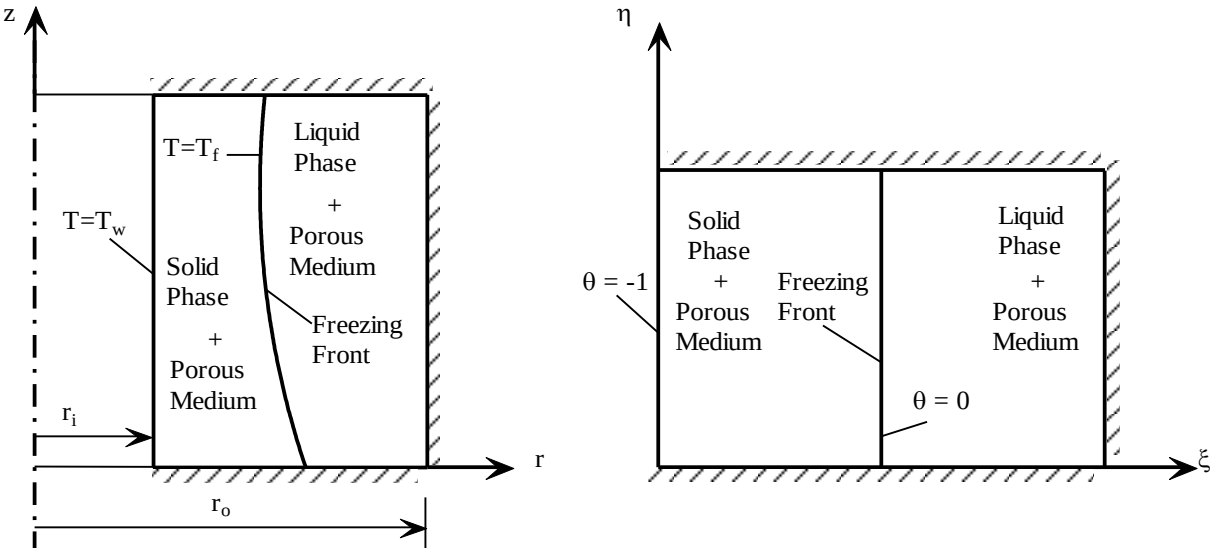

Fig. (3) Schematic diagram for the physical model, coordinate systems and boundary conditions

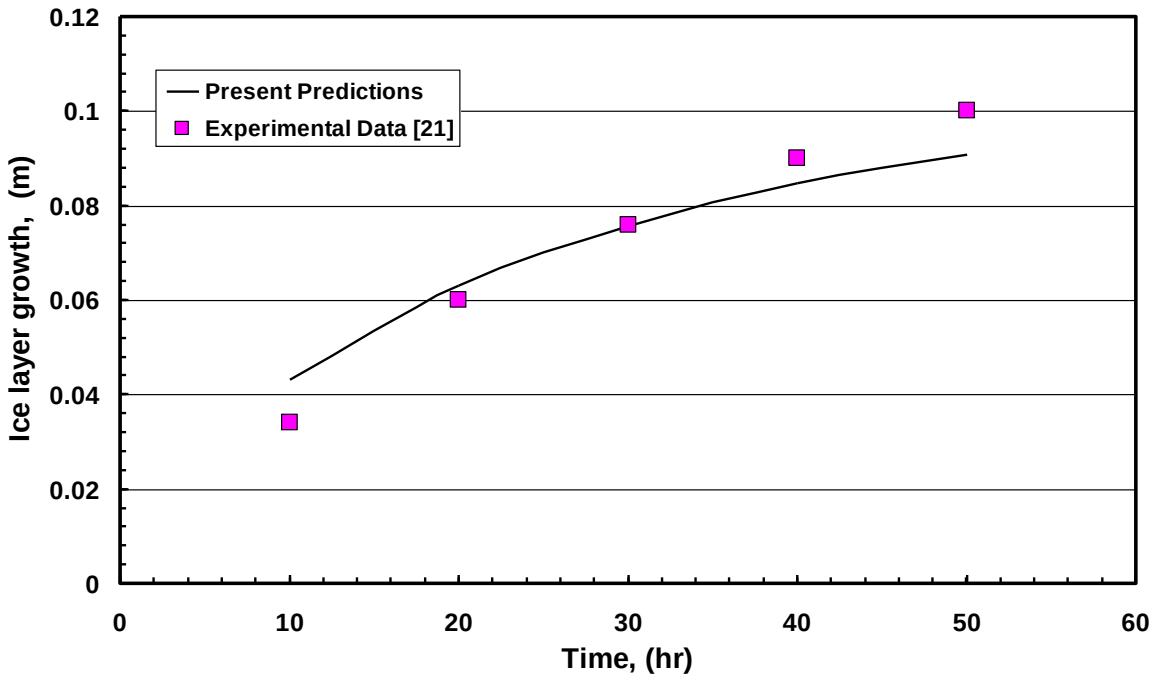

Fig. (4) Comparison of the present model predictions with the experimental data, [21]

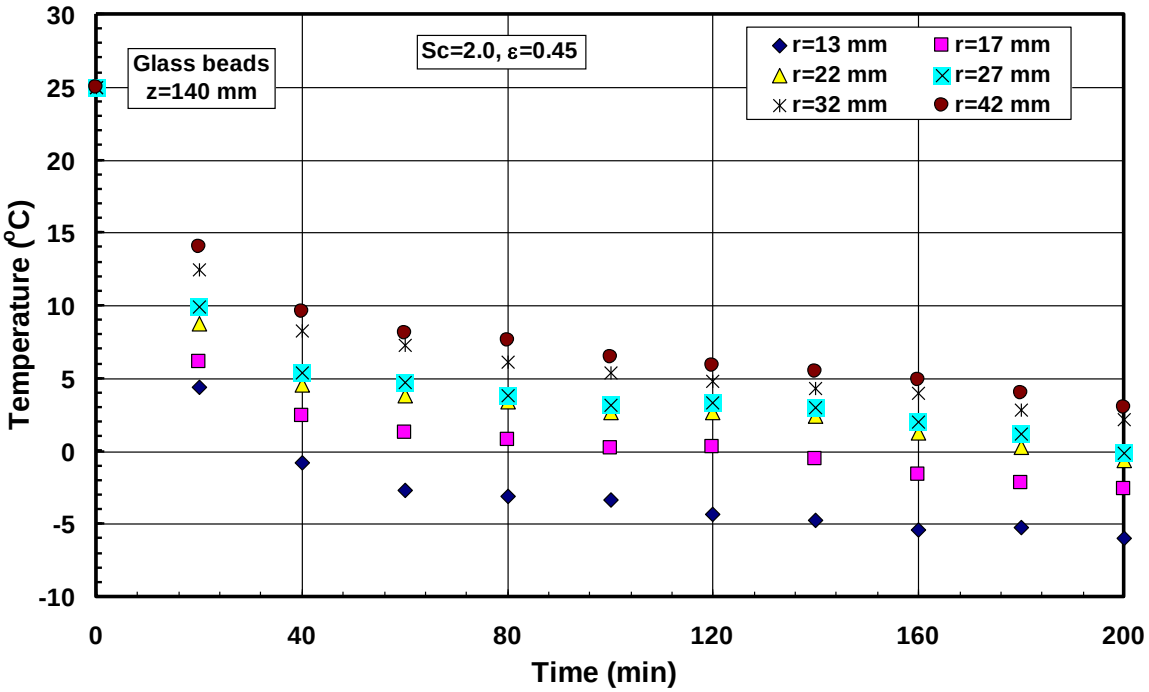

Fig. (5) Timewise variation of temperature at different radial location for water saturated-glass beads

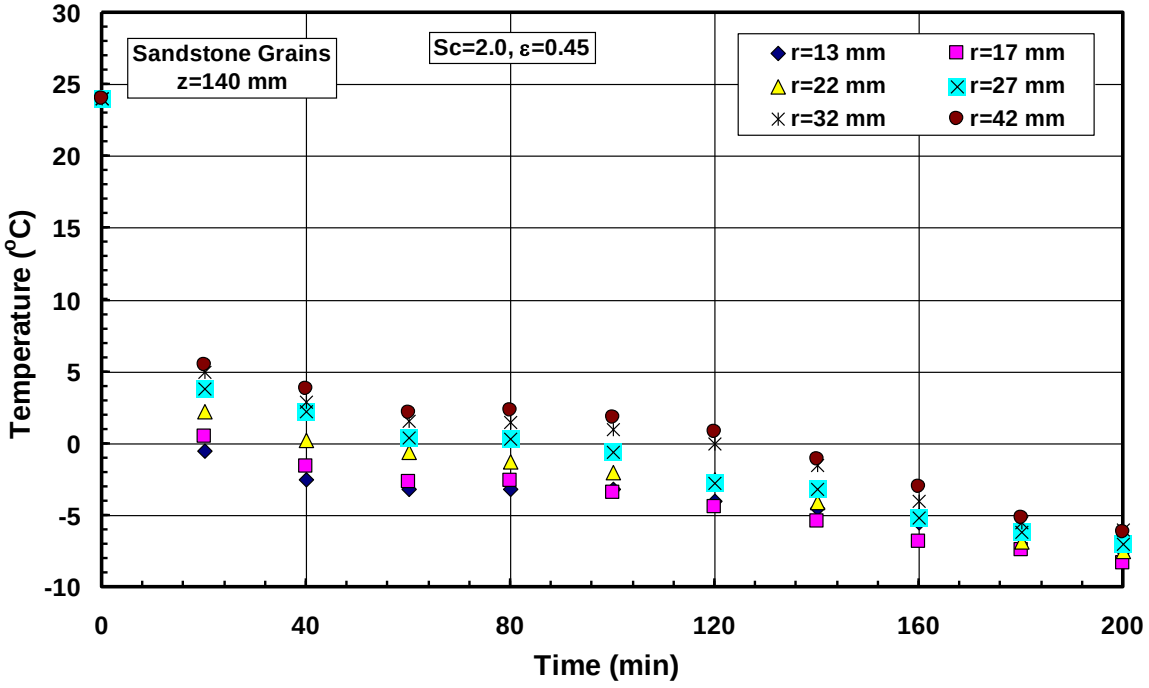

Fig. (6) Timewise variation of temperature at different radial location for water saturated-sandstone grains

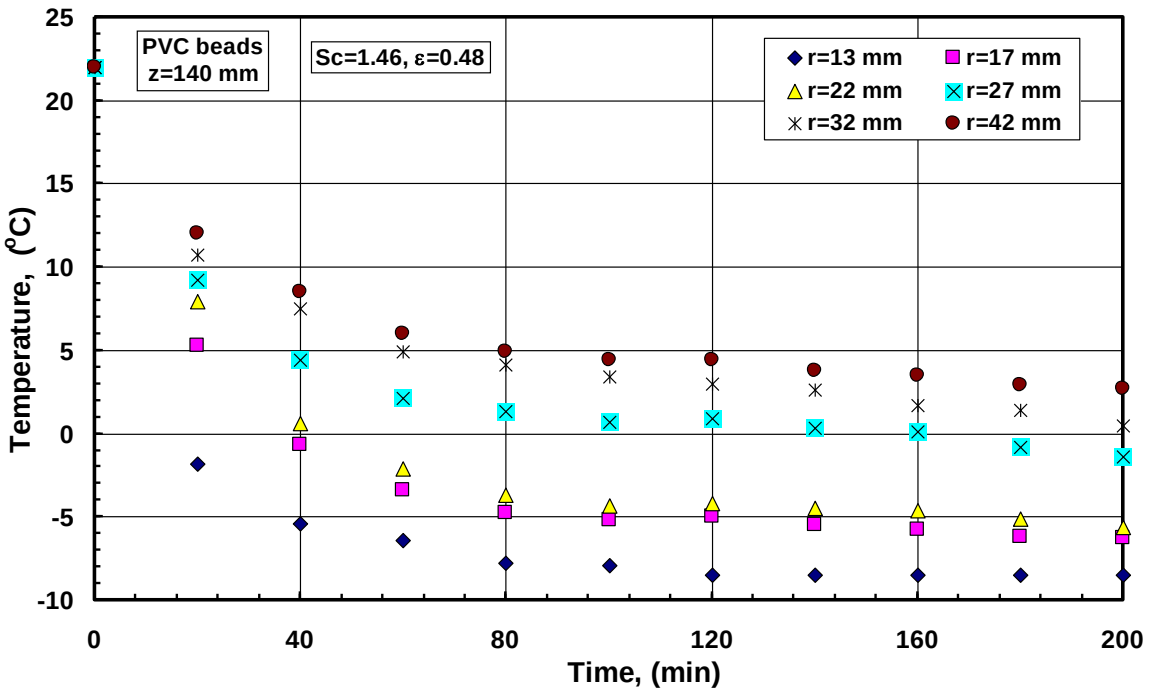

Fig. (7) Timewise variation of temperature at different radial location for water saturated-PVC beads

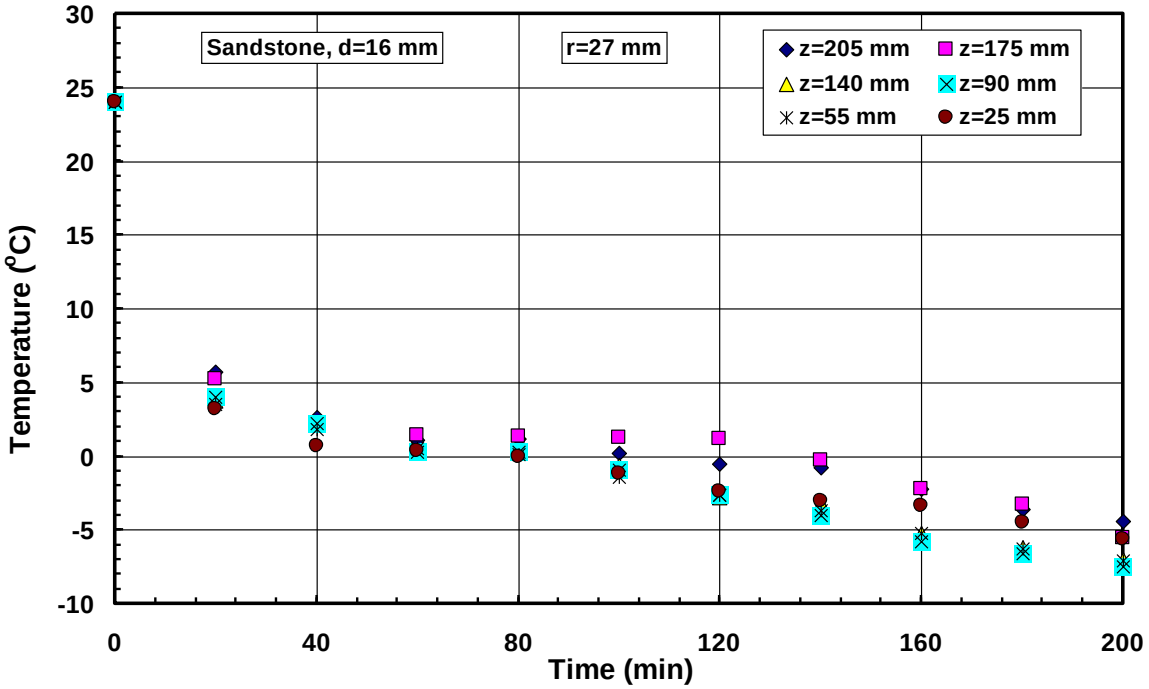

Fig. (8) Timewise variation of temperature at different axial location for water saturated-sandstone grains

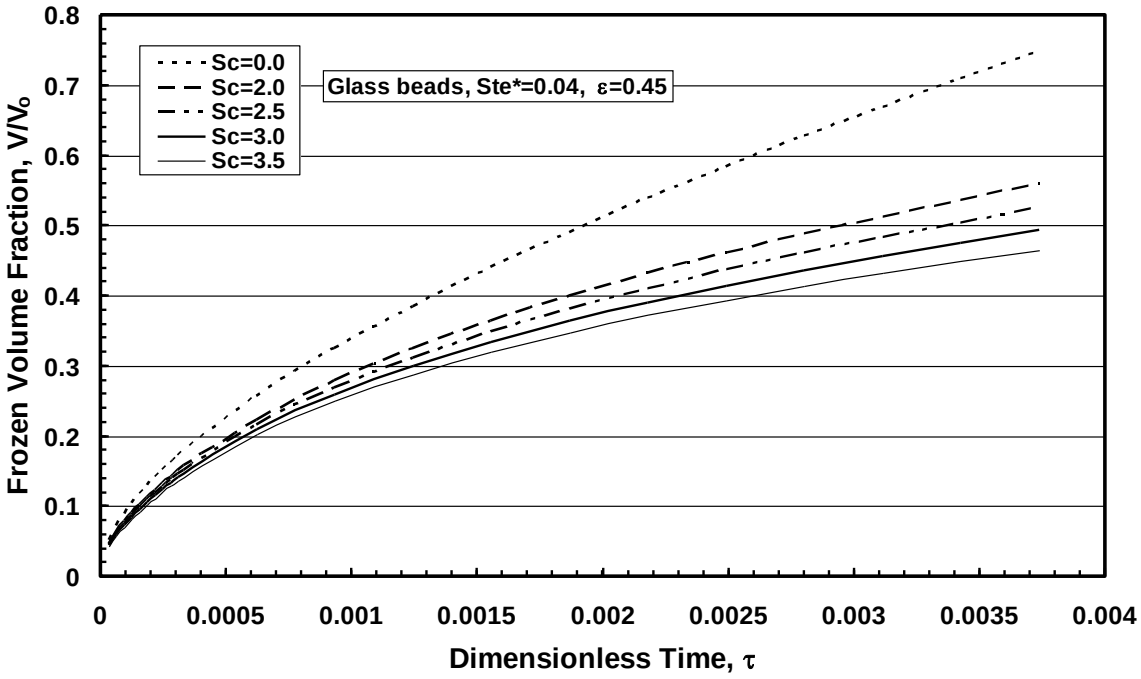

Fig. (9) Timewise variation of frozen volume fraction for glass beads at different initial liquid superheating coefficient (initial liquid temperature)

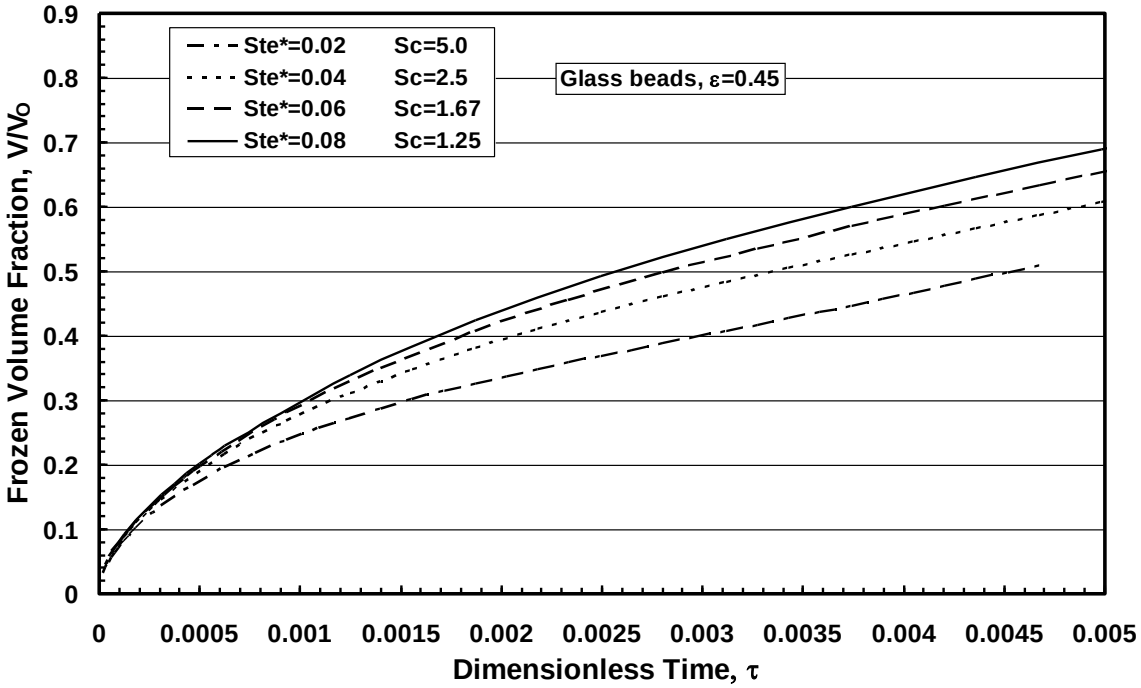

Fig. (10) Timewise variation of frozen volume fraction for glass beads at different Stefan number (cold inner tube temperature)

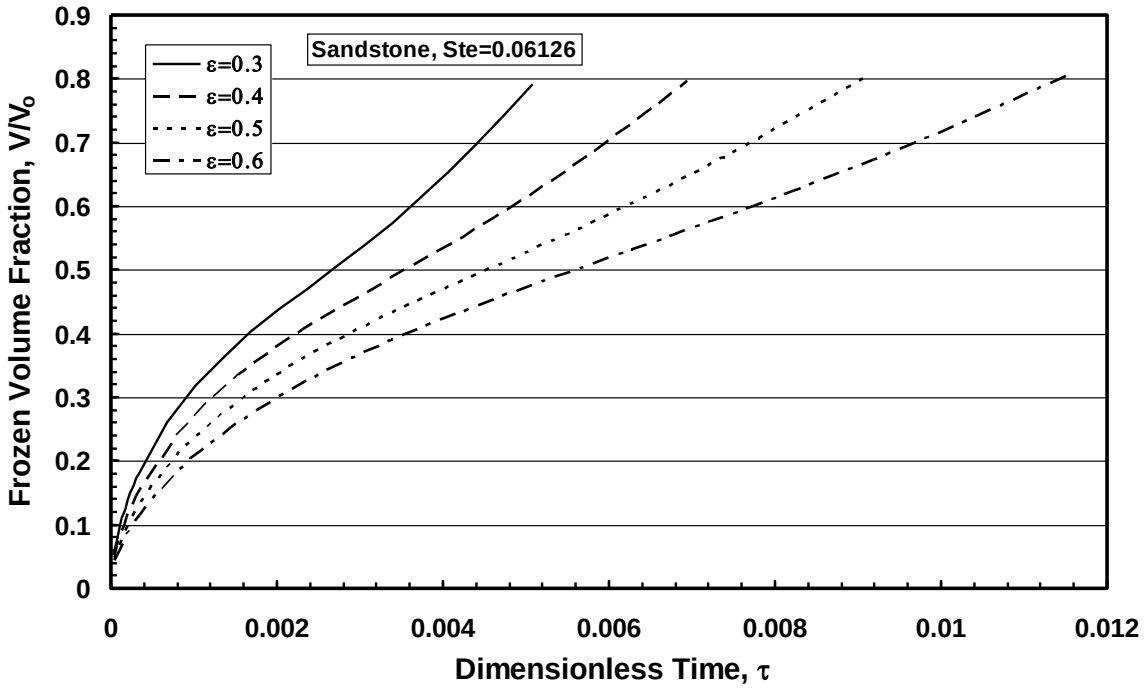

Fig. (11) Timewise variation of frozen volume fraction for sandstone grains at different porosity

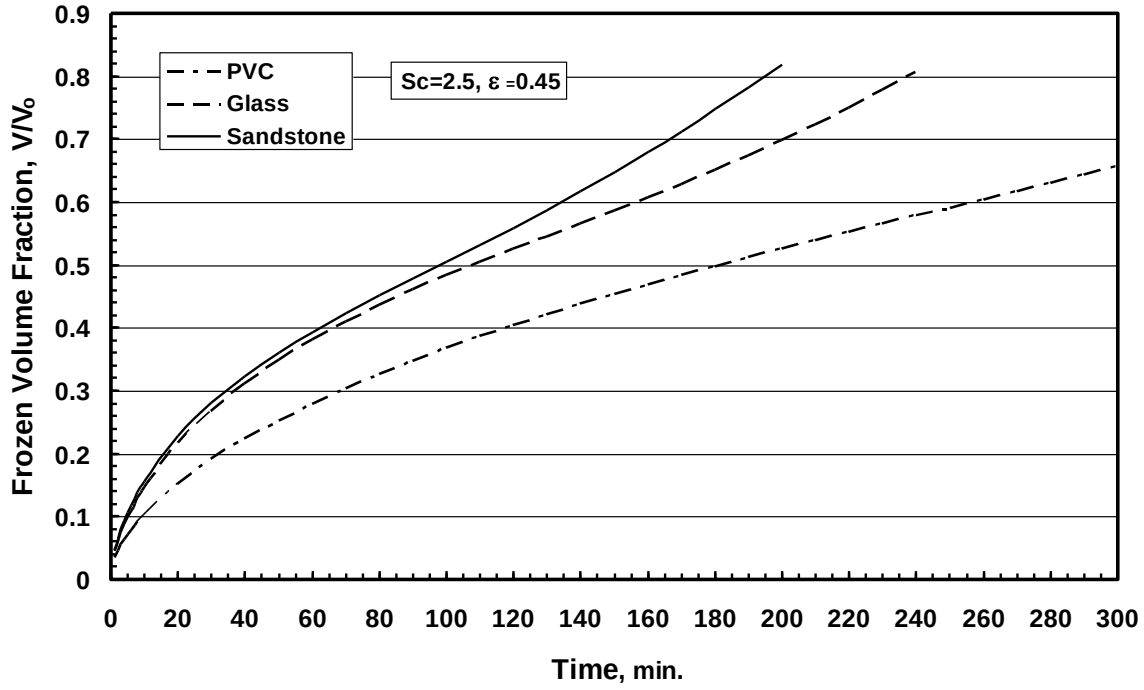

Fig. (12) Timewise variation of frozen volume fraction for different porous materials

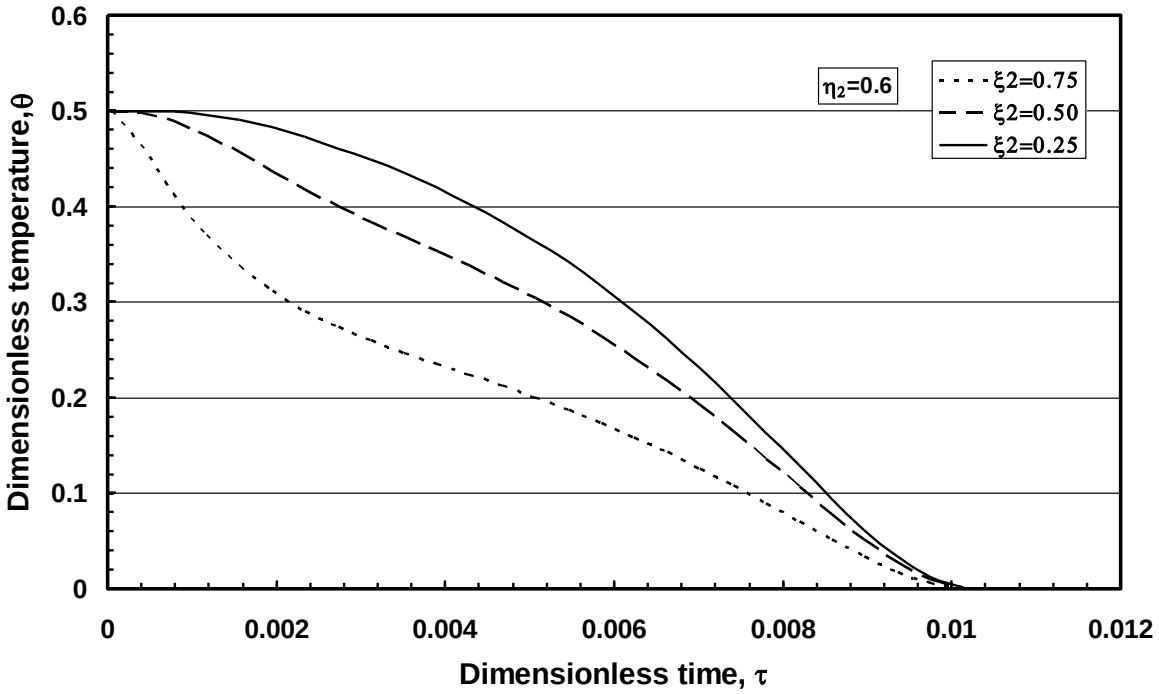

Fig. (13) Timewise variation of dimensionless temperature at different radial locations for liquid phase-PVC beads, at ε=0.475, Sc=1.47, Ste=0.066

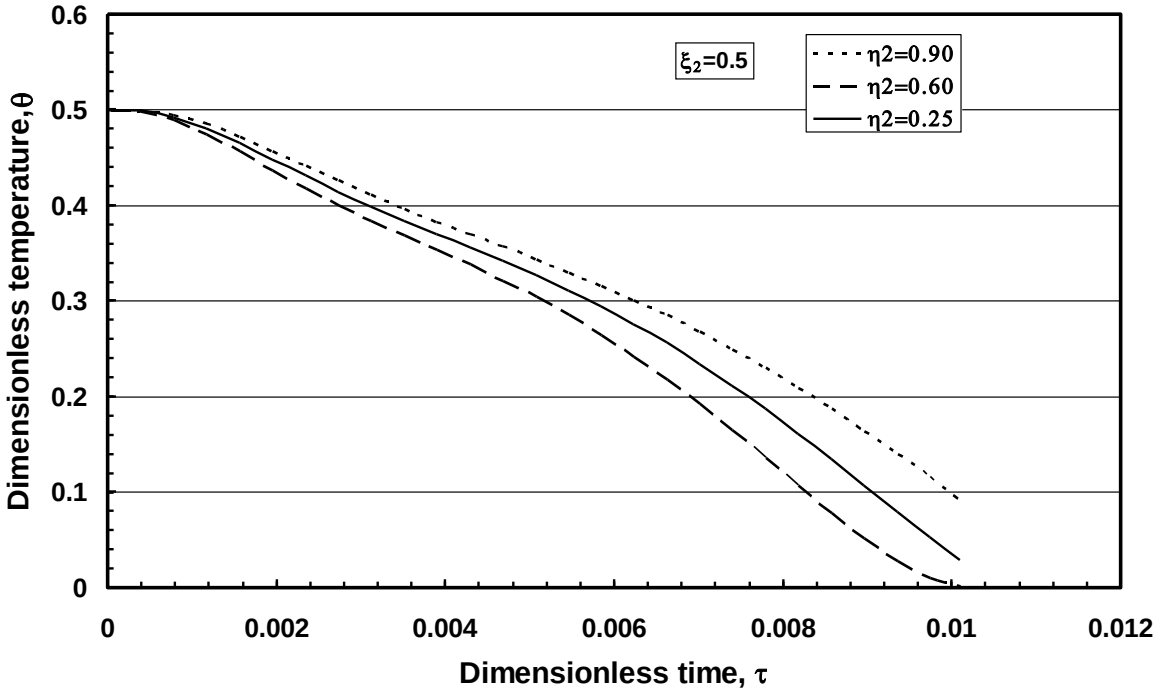

Fig. (14) Timewise variation of dimensionless temperature at different axial locations for liquid phase-PVC beads at ε=0.475, Sc=1.47, Ste=0.066

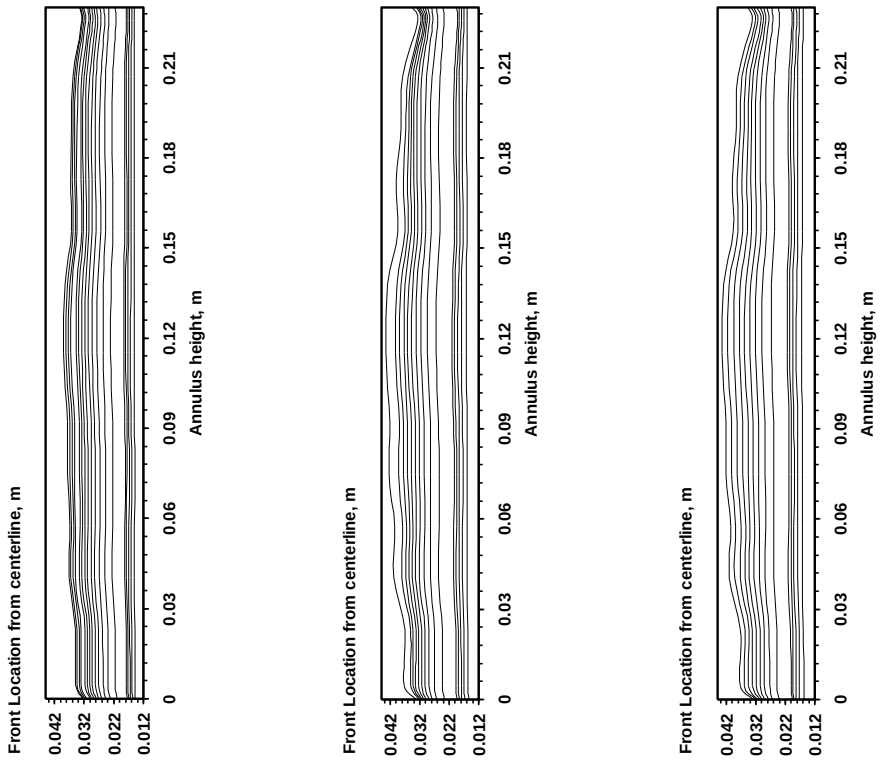

(a) PVC beads (a) Glass beads (a) Sandstone grains

Fig. (15) Freezing front location for water saturated different porous materials; Sc=2.5, ε=0.45, Time interval between lines is 20 min.

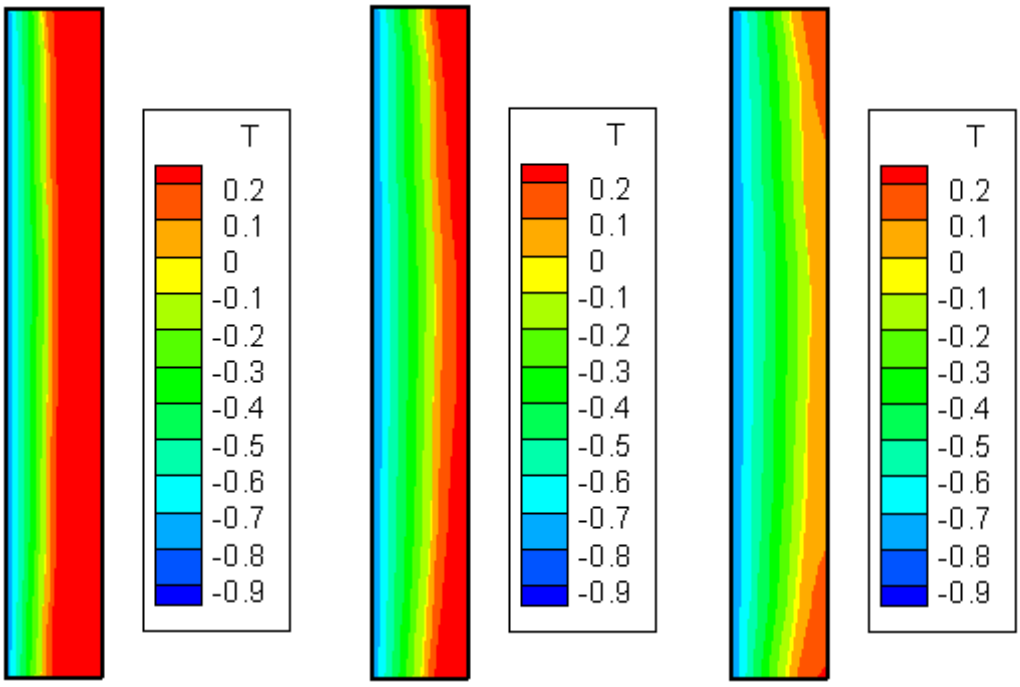

(a) t=30 min. (a) t=90 min. (a) t=150 min.

Fig. (16) Temperature contours for water saturated sandstone grains undergoing freezing process at different times, Sc=0.45 and ε=0.45

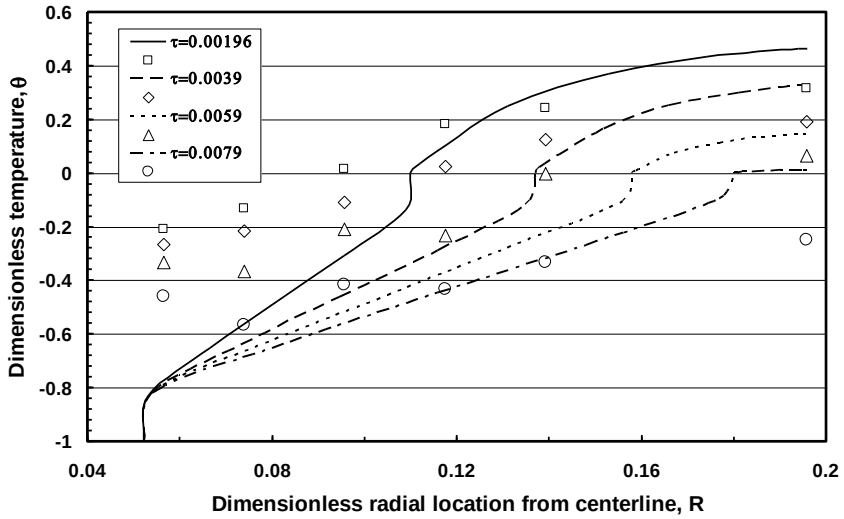

Fig. (17) Comparison of the predicted and measured temperature for freezing water saturated-sandstone grains at ε=0.45, Sc=2.0, Ste*=0.047

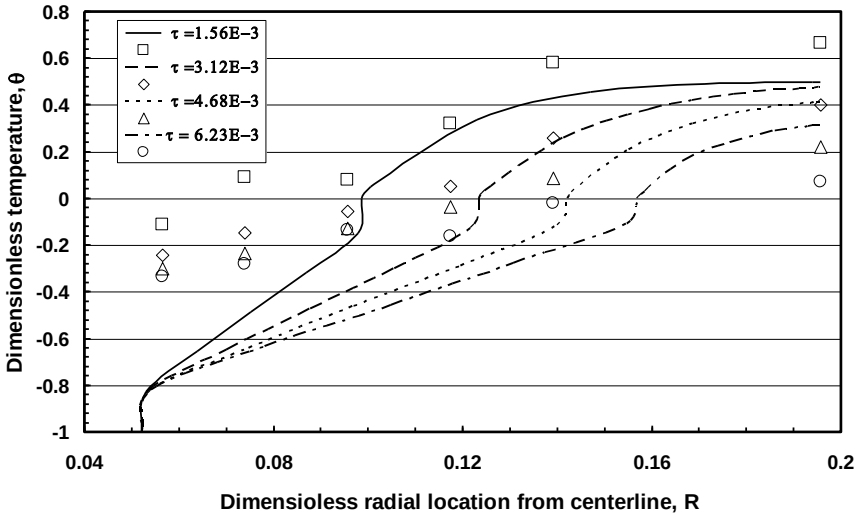

Fig. (18) Comparison of the predicted and measured temperature for freezing water saturated-PVC beads at ε=0.475, Sc=1.47, Ste=0.066

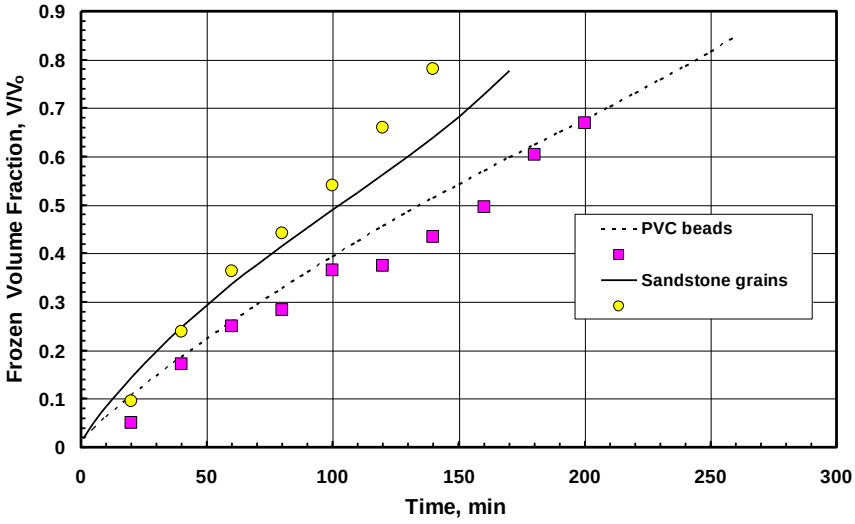

Fig. (19) Comparison of the predicted and measured frozen volume fraction for freezing water saturated-sandstone grains at □ε=0.45, Sc=2.0, Ste*=0.047 and PVC beads at ε=0.475, Sc=1.47, Ste=0.066